APPENDIX - RESULTS OBTAINED TO DATE

Joanne L. Walsh, Aditi Chattopadhyay,

Jocelyn I. Pritchard, and Mark W. Nixon

To date, progress has been made in the areas of aerodynamic performance optimization, dynamic optimization, optimum placement of tuning masses for vibration reduction, and structural optimization. Selected results from these activities are highlighted in this appendix.

Results - Aerodynamic Performance Optimization

This section of the paper describes the application of formal mathematical programming to optimization of the aerodynamic performance of rotor blades. This work is described in detail in reference 9.

A previous analytical procedure for designing rotor blades, referred to herein as the conventional approach (ref. 46) served as the starting point for the development of the method in reference 9. The method of reference 46 combined a momentum strip theory analysis for hover (HOVT) based on reference 17 and the Rotorcraft Flight Simulation computer program (C-81, ref. 47) for forward flight. The program HOVT was used to compute hover horsepower. The program, C-81, (quasi-static trim option) was used to define the trim condition, the horsepower required, and the airfoil section drag coefficients for forward flight and maneuver conditions. Both analyses used experimental two-dimensional airfoil data.

The mathematical optimization formulation in reference 9 can be stated in terms of a design goal and a set of design requirements. The design goal is to reduce the hover horsepower for a given helicopter with a specified design gross weight operating at a specified altitude and temperature. Satisfactory forward flight performance is defined by the following three requirements. First, the required horsepower must be less than the available horsepower. Second, airfoil section stall along the rotor blade must be avoided, i.e., the airfoil sections distributed along the rotor blade

must operate at section drag coefficients less than a specified value neglecting the large drag coefficients in the reverse flow region. Third, the helicopter must be able to sustain a simulated pull-up maneuver, i.e., the aircraft must operate trimmed at a gross weight equal to a specified multiple (load factor) of the design gross weight for a second specified horizontal velocity V_{lf}.

In reference 9, the airfoil selection and distribution were preassigned. The design parameters point of taper initiation, root chord, taper ratio, and maximum twist - are illustrated in figure 13. The point of taper initiation, r, is the radial station where taper begins. The blade is rectangular up to this station and then tapered linearly to the tip. The taper ratio, TR, is c_r/c_t where c_r is the root chord and c_t is the tip chord. The twist varies linearly from the root to the tip where the maximum value τ_{max} occurs. The approach uses the same rotor blade performance analyses as reference 46, but couples a general-purpose optimization program to the analyses. Using this approach, the user is less involved in manipulating the design variables as he would be using the conventional approach. Instead, the optimization program takes over the role of manipulating the design variables to arrive at the best blade design.

In reference 9 the mathematical programming approach was used to obtain rotor blade designs for three Army helicopters - the AH-64, the UH-1, and a conceptual high-speed performance helicopter. In each case the goal was to find, for preselected rotor speed, rotor blade radius, airfoil sections and distribution, the blade configuration which has the lowest hover horsepower for a given design gross weight and a selected pull-up maneuver. Results obtained in references 9 and 44 for the AH-64 helicopter are presented here.

The final AH-64 rotor blade designs obtained using both the conventional and mathematical programming approaches are shown in figure 14. Results include the final design variable values, the main rotor horsepowers required for hover (the objective function), for forward flight, and for the simulated pull-up maneuver

conditions, for each approach. The mathematical programming approach produces a design which had more twist, a point of taper initiation further outboard, and a smaller blade root chord than the conventional approach. The mathematical programming design requires 25 fewer horsepower in hover than the conventional design. Most significantly, mathematical programming approach obtained results about 10 times faster than the conventional approach (2 days vs. 5 weeks).

Results - Dynamic Optimization Through Frequency Placement

One important dynamics design technique is to separate the natural frequencies of the blade from the harmonics of the airloads to avoid resonance. This can be done by a proper tailoring of the blade stiffness and mass distributions. This section of the paper describes a procedure developed in reference 7.

Minimum weight designs of helicopter rotor blades with both rectangular and tapered planforms have been obtained subject to the following constraints: (a) upper and lower bounds ("windows") on the frequencies of the first three elastic lead-lag dominated modes and the first two elastic flapping dominated modes, (b) minimum prescribed value of blade autorotational inertia, and (c) upper limit on the blade centrifugal stress. Side constraints have been imposed on the design variables to avoid impractical solutions.

Design variables (fig. 15) include blade taper ratio, dimensions of the box beam located inside the airfoil section, and magnitudes of the nonstructural masses. The program CAMRAD has been used for the blade modal analysis and the program CONMIN has been used for the optimization. In addition, a linear approximation involving Taylor series expansion has been used to reduce the analysis effort. The procedure contains a sensitivity analysis which produces analytical derivatives of the objective function, the autorotational inertia constraint, and the stress constraints. A central finite difference scheme has been used for the derivatives of the frequency constraints.

The optimization process begins with an arbitrary set of design variable values. The mathematical formulation of the optimization problem is presented in figure 16. The blade weight W has two components W_b (structural weight) and W_o (nonstructural weight) and is expressed in the discretized form in figure 16, where N denotes the total number of segments and ρ_j, A_j, L_j, and W_{o_j} denote the density, the cross sectional area, the length, and the nonstructural weight of the jth segment, respectively. The subscripts L and U refer to the respective lower and upper bounds, σ_k is the centrifugal stress in the kth segment, M_j is the total mass of the jth segment, and Ω is the blade rpm. The quantity FS denotes a factor of safety and σ_{max} is the maximum allowable blade stress.

The reference blade (refs. 5 and 7) shown in figure 15 is articulated and has a rigid hub. The blade has a rectangular planform, a pretwist, and a root spring which allows torsional motion. A box beam with unequal vertical wall thicknesses is located inside the airfoil. As in reference 5, it is assumed that only the box beam contributes to the blade stiffness, that is, contributions of the skin, honeycomb, etc. to the blade stiffness are neglected. For the rectangular blade, the box beam is modeled by ten segments and is uniform along the blade span. For the tapered blade, the box beam is tapered and is modeled by ten segments. A linear variation of the box beam height, h, in the spanwise direction has been assumed.

Table 5 presents a summary of the optimization results for the rectangular blade with 30 design variables (three box beam dimensions at ten segments) and the tapered blade with 42 design variables (30 box beam dimensions, 10 segment masses, taper ratio, and root chord). The optimum rectangular blade is 2.67 percent lighter than the reference blade and the optimum tapered blade is 6.21 percent lighter than the reference blade. The optimum tapered blade has a taper ratio (λ_h) of 1.49. The first lead-lag frequency (f_1) is at its prescribed upper bound after optimization and the autorotational inertia is at its lower bound for all cases. Additional results along with optimum design variable distributions can be found in reference 7 which

also discusses the effect of higher frequency constraints and stress constraints on the optimum blade weight and design variable distributions.

Results - Optimum Locations of Vibration Tuning Masses

The objective of this work is to develop and demonstrate a method for optimally locating, as well as sizing, tuning masses to reduce vibration using formal mathematical optimization techniques. The design goal is to find the best combination of tuning masses and their locations to minimize blade root vertical shear without a large mass penalty. The method is to formulate and solve an optimization problem in which the tuning masses and their locations are design variables that minimize a combination of vertical shear and the added mass with constraints on frequencies to avoid resonance. Figure 17 shows an arbitrary number of masses placed along the blade span. Two alternate optimization strategies have been developed and demonstrated. The first is based on minimizing the amplitudes of the harmonic shear corresponding to several blade modes. The second strategy reduces the total shear as a function of time during a revolution of the blade. Results are shown in which the above strategies are applied to a rotor blade considering multiple blade mode/ multiple harmonic airload cases.

The example problem is a beam representation of an articulated rotor blade. The beam is 193 inches long with a hinged end condition and is modeled by 10 finite elements of equal length. The model contains both structural mass and lumped (non-structural) masses. Three lumped masses are to be placed along the length of the beam. The first strategy was applied to minimize the 4/rev blade root vertical shear response S_4 of the first and second elastic flapping modes without using excessive tuning mass. Figure 18 summarizes the initial and final designs. The initial shear amplitude is 34.68 lbf which is reduced by the optimization process to 0.01 lbf with an accompanying decrease in the tuning mass. The second strategy was applied to a test case of two modes responding to three harmonics of airload. Figure 19 shows for

the initial and final designs, the shear s(t) plotted as a function of the time and azimuth for a revolution of the blade. The peaks on the initial curve have been reduced dramatically. For example, the maximum peak s_{max} for the initial design is 78.00 lbf, and for the final design, the maximum peak is 0.576 lbf.

Results - Rotor Structural Optimization

A blade structural optimization procedure (fig. 20) applicable to metal and composite blades has been developed in which the objective function is blade mass with constraints on frequencies, stresses in the spars and in the skin, twist deformation, and autorotational inertia. The design variables are the total spar thickness and for the composite blade the percentage of $\pm 45^{\circ}$ plies (the remaining plies assumed to be at 0°). This procedure is described in detail in reference 10, and additional applications of the methods are also given in reference 10.

This section describes two example rotor blade designs which were developed using the structural design methodology. Both designs are based on the UH-60 Black Hawk titanium spar blade. The first design case is for a titanium single spar cross section. This design was conducted to validate the present design methodology. The second case has a graphite/epoxy spar in a single spar cross-section configuration. The composite spar design is compared to the metal spar design to explore potential weight savings obtained from use of the design methodology in conjunction with composite materials.

Titanium cross section.- A titanium spar blade design was developed using the previously described design methodology. The cross-section model was based on the UH-60 rotor blade with identical skin, core, trailing edge tab, leading edge weight, and spar coordinates. Only the spar thickness was used as a design variable. The beam model representation of the blade used a rectangular planform similar to the UH-60 planform, but without any tip sweep. A maximum twist of deformation of 3.1° is based on an aerodynamic performance constraint (ref. 10). The structural constraint

requires that the calculated stresses do not exceed the allowable material strength. The material strength is assessed by use of a Tsai-Hill failure criterion based on the associated margins of safety. The margins of safety must be greater than zero to satisfy the material strength constraint. The autorotation capability is assumed to be the same for this design as it is for the UH-60. Autorotation is satisfied by requiring the mass moment of inertia to be identical to that of the UH-60 rotor system which is 19000 in-lbs-s per blade. Before a comparison to the UH-60 blade can be made, the design must be dynamically tuned. The modes considered in this design are first elastic flapwise and edgewise bending, first torsion, and second and third flapwise bending. The frequencies of these modes are required to be removed from integer multiples of the forcing frequency by 0.2 per rev.

As shown in figure 21, the minimum spar thickness needed to satisfy all the constraints is 0.130 inch which corresponds to a blade weight of 207 pounds. The actual UH-60 titanium spar is 0.135 inch thick, producing a 210 pound blade. The titanium spar design is only 3 pounds different from the actual UH-60 blade, demonstrating that the mechanics of the design methodology can produce blade designs similar to conventional design processes. The only significant difference in modal frequencies between the actual UH-60 blade and the titanium spar design is the frequency of the torsional mode. The difference is attributed to the chordwise distribution of the nonstructural tip weight which, in the present titanium spar design, was lumped at the chordwise c.g.

Composite cross section.- A second design was developed using a single T300-5208 graphite/epoxy D-spar. The blade models and associated design assumptions used in the composite design were the same as those used for the metal spar except for the spar material. Here, thickness and ply orientation of the composite spar were used as design variables. The plies of the spar were assumed to consist only of 0° and $\pm 45^\circ$ angles symmetrically built up. Thus, the ply orientation design variable was the percentage of $\pm 45^\circ$ plies in the laminate. The remaining plies of the laminate

are understood to be oriented at 0°. Constraints on twist deformation, material strength, mass moment of inertia, and dynamic tuning are the same as those used for the metal design.

Results shown in figure 21 show that the composite design satisfied the required constraints. Further, the minimum weight design had a 0.105 inch thick spar with 20 percent of the plies oriented at $\pm 45^{\circ}$ degrees which resulted in blade weight savings of 21.5 percent. These results demonstrate that this design methodology, used in conjunction with composite materials, can result in significant weight savings.

REFERENCES

1. Ashley, H.: On Making Things the Best - Aeronautical Use of Optimization. AIAA Journal of Aircraft, vol. 19, no. 1, 1982.

2. Sobieszczanski-Sobieski, J.: Structural Optimization Challenges and Opportunities. Presented at International Conference on Modern Vehicle Design Analysis, London, England, June 1983.

3. Miura, H.: Application of Numerical Optimization Methods to Helicopter Design Problems: A Survey. NASA TM-86010, October 1984.

4. Bennett, R. L.: Application of Optimization Methods to Rotor Design Problems. Vertica, vol. 7, no.3, 1983, pp. 201-208.

5. Peters, D. A.; Rossow, M. P.; Korn, A.; and Ko, T.: Design of Helicopter Rotor Blades for Optimum Dynamic Characteristics. Computers and Mathematics With Applications, vol. 12A, no. 1, 1986, pp. 85-109.

6. Friedmann, P.: Application of Modern Structural Optimization to Vibration Reduction in Rotorcraft. Vertica, vol. 9, no. 4, 1986, pp. 363-376.

7. Chattopadhyay, Aditi; and Walsh, Joanne L.: Minimum Weight Design of Rotorcraft Blades With Multiple Frequency and Stress Constraints. Proceedings of the AIAA/ASME/ASCE/AHS 29th Structures, Structural Dynamics and Materials Conference, Williamsburg, VA, April 18-20, 1988. AIAA Paper No. 88-2337-CP. Also available as NASA TM-100569, March 1988.

8. Davis, M. W.: Optimization of Helicopter Rotor Blade Design for Minimum Vibration. NASA CP-2327, Part 2, September 1984, pp. 609-625.

9. Walsh, J. L.; Bingham, G. J.; and Riley, M. F.: Optimization Methods Applied to the Aerodynamic Design of Helicopter Rotor Blades. Journal of American Helicopter Society, October 1987, pp. 39-44.

10. Nixon, M. W.: Preliminary Structural Design of Composite Main Rotor Blades for Minimum Weight. NASA TP-2730, July 1987.

11. Rao, S. S.: Multiobjective Optimization in Structural Design with Uncertain Parameters and Stochastic Processes. AIAA Journal, Vol. 22, No. 11, November 1984.

12. Vanderplaats, G. N.: CONMIN - A Fortran Program for Constrained Function Minimization. User's Manual. NASA TMX-62282. August 1973.

13. Sobieszczanski-Sobieski, J.: On the Sensitivity of Complex, Internally Coupled Systems. NASA TM-100537, January 1988.

14. Johnson, Wayne: A Comprehensive Analytical Model of Rotorcraft Aerodynamics and Dynamics. NASA TM 81182, 1980.

15. Walsh, Joanne L.: Applications of Numerical Optimization Procedures to a Structural Model of a Large Finite-Element Wing. NASA TM 87597, 1986.

16. Bingham, Gene J.: The Aerodynamic Influences of Rotor Blade Airfoil, Twist, Taper, and Solidity on Hover and Forward Flight Performance. 37th Annual Forum of the American Helicopter Society. New Orleans, Louisiana, May 1981.

17. Gessow, Alfred; and Myers, Garry C., Jr.: Aerodynamics of the Helicopters. Frederick Unger Publishing Company, New York, 1952.

18. Strawn, Roger C.; and Tung, Chee: Prediction of Unsteady Transonic Rotor Loads With A Full-Potential Rotor Code. 43rd Annual Forum of the American Helicopter Society. St. Louis, Missouri, May 1987.

19. Berry, John D.: Quarter Scale Testing of an Advanced Rotor System for the UH-1 Helicopter. 37th Annual Forum of the American Helicopter Society. New Orleans, Louisiana, May 1981.

20. Kelley, Henry L.; and Wilson, John C.: Aerodynamic Performance of a 27-Percent-Scale AH-64 Wind-Tunnel Model With Baseline/ Advanced Rotor Blades. 41st Annual Forum of the American Helicopter Society. Ft. Worth, Texas, May 1985.

21. Kelley, Henry L.: Effect of Planform Taper on Hover Performance of an Advanced AH-64 Model rotor. NASA TM 89145, 1987.

22. Yeager, W. T.; Mantay, W. R.; Wilbur, M. L.; Cramer, R. G., Jr.; and Singleton, J. D.: Wind-Tunnel Evaluation of an Advanced Main-Rotor Blade Design for a Utility-Class Helicopter. NASA TM 89129, 1987.

23. Pritchard, J. I.; and Adelman, H. M.: Optimal Placement of Tuning Masses for Vibration Reduction in Helicopter Rotor Blades. Presented at the Second International Conference on Rotocraft Basic Research, College Park, Md., February 1988.

24. Whetstone, W. D.: EISI-EAL Engineering Analysis Language Reference Manual. Engineering Information Systems, Inc., San Jose, CA, 1983.

25. Jones, Robert M.: Mechanics of Composite Materials. Scripta Book Co., Washington, DC, 1975.

26. MIL-S-8698, Structural Design Requirements, Helicopters, August 1950.

27. Department of the Army: Engineering Design Handbook, Helicopter Engineering, Part One, Preliminary Design. AMC PAMPHLET No. 706-201, August 1974.

28. Brentner, K. S.: Prediction of Helicopter Rotor Discrete Frequency Noise - A Computer Program Incorporating Realistic Blade Motions and Advanced Acoustic Formulation. NASA TM-87721, October 1986.

29. Ffowcs Williams, J. E.; and Hawkings, D. L.: Sound Generation by Turbulence and Surfaces in Arbitrary Motion. Philos. Trans. R. Soc. London, ser. A, vol. 264, no. 1151, May 8, 1969, pp. 321-342.

30. Lighthill, M. J.: On Sound Generated Aerodynamically. I. General Theory. Proc. R. Soc. (London), ser. A, vol. 211, no. 1107, Mar. 20, 1952, pp. 564-587.

31. Farassat, F.; and Succi, G. P.: The Prediction of Helicopter Rotor Discrete Frequency Noise. Vertica, vol. 7, no. 4, 1983, pp. 309-320.

32. Farassat, F.: Theory of Noise Generation From Moving Bodies With an Application to Helicopter Rotors. NASA TR R-451, 1975.

33. Farassat, F.: Advanced Theoretical Treatment of Propeller Noise. Propeller Performance and Noise, VKI-LS 1982-08, Volume 1, Von Karman Inst. Fluid Dyn., May 1982.

34. Coleman, R. P.; and Feingold, A. M.: Theory of Self-Excited Mechanical Oscillations of Helicopters With Hinged Blades. NACA Report 1351, 1958.

35. Donham, R. E.; Cardinale, S. V.; and Sachs, I. B.: Ground and Air Resonance Characteristics of a Soft-Inplane Rigid-Rotor System. Journal of the American Helicopter Society, vol. 14, no. 4, October 1969, pp. 33-41.

36. Wood, E. R.; and Buffalano, A. C.: Parametric Investigation of the Aerodynamic and Aeroelastic Characteristics of Articulated and Rigid (Hingeless) Helicopter Rotor Systems. U.S. Army TRECOM Technical Report 64-15, April 1964.

37. Gerstenberger, W.; and Wood, E. R.: Analysis of Helicopter Aeroelastic Characteristics in High-Speed Flight. AIAA J., vol. 1, no. 10, Oct. 1963, pp. 2366-2381.

38. Novak, M. E.: Rotating Elements in the Direct Stiffness Method of Dynamic Analysis With Extensions to Computer Graphics. Shock and Vibration Bulletin, Bull. 40, Pt. 4, Oct. 1969, pp. 41-46.

39. Staley, J. A.; and Sciarra, J. J.: Coupled Rotor/Airframe Vibration Prediction Methods. Rotorcraft Dynamics, NASA SP-352, 1974, pp. 81-90.

40. Berry, J. D.; et al.: Helicopter Rotor Induced Velocities Theory and Experiment. American Helicopter Society Specialists Meeting on Aerodynamics and Aeroacoustics, February 1987.

41. Caradonna, F. X.; Lautenschlager, J. L.; and Silva, M. J.: An Experimental Study of Rotor-Vortex Interactions. Preprint from AIAA 26th Aerospace Sciences Meeting, January 1988.

42. Lake, R. C.; and Nixon, M. W.: Results From a Preliminary Investigation of Finite-Element Modeling in Analysis of Composite Rotor Blades. Second International Conference on Rotorcraft Basic Research, February 1988.

43. Althoff, S. L.: Effect of Advanced Rotorcraft Airfoil Sections on the Hover Performance of a Small Scale Rotor Model. NASA TP-2832 (AVSCOM TP-88-B-001) Sept. 1988.

44. Gardner, J. E.; and Dixon, S. C.: Loads and Aeroelasticity Division Research and Technology Accomplishments for FY 1984 and Plans for FY 1985. NASA TM 86356, 1985, pp. 138-139.

45. Mantay, W. R.; and Rorke, J. B.: The Evolution of the Variable Geometry Rotor. American Helicopter Society Symposium on Rotor Technology Proceedings, August 1976.

46. Bingham, Gene J.: The Aerodynamic Influences of Rotor Blade Taper, Twist, Airfoils and Solidity on Hover and Forward Flight Performance. 37th Annual Forum of the American Helicopter Society. New Orleans, Louisiana, May 1981.

47. Van Gaasbeck, J. R.: Rotorcraft Flight Simulation, Computer Program C81. USARTL-TR-77-54B, 1979.

TABLE 1.- SUMMARY OF DESIGN VARIABLES

Description	Symbol
Tuning mass at location i	m_i
Spanwise location of i-th mass	x_i
Wing box dimensions	t_1, t_2, t_3
Ply thicknesses	t_{45}, t_o
Depth of blade at root	h_r
Ratio of blade depths at tip and root	$\lambda_h = h_r/h_t$
Maximum pre-twist of blade	τ_{max}
Percent blade span where taper begins	r
Blade root chord	c_r
Airfoil distribution	-
Hinge offset	e
Blade angular velocity	Ω
Number of blades on rotor	N
Blade radius	R
Ratio of root chord to tip chord	$\lambda_c = c_r/c_t$

TABLE 2.- SUMMARY OF CONSTRAINTS

Constraint Description	Form of Constraint	Comments
Main rotor horsepower	$HP_i \leq$ HP avail for i-th condition	For 5 flight conditions Enforced at 12 azimuthal locations
Airfoil section stall	$C_D \leq C_{Dmax}$	
Blade frequencies	$f_{i\ell} \leq f_i \leq f_{iu}$	
Blade vertical load	$V_{ik} \leq V_{max}$	
Blade inplane load	$H_{ik} \leq H_{max}$	
Transmitted in-plane hub shears	$X_k \leq X_{max}$ $Y_k \leq Y_{max}$	
Hub pitching moment	$P_k \leq P_{max}$	
Hub rolling moment	$R_k \leq R_{max}$	
Blade response amp.	$q_k \leq Q_{max}$	
Autorotational inertia	$\Sigma m \cdot {}^2 \geq \alpha$	
Aeroelastic stability	Re $\leq -\epsilon$	
Wing box stresses	$R \leq 1$	R = TSai-Hill criterion
Blade tip deflection	$w \leq w_{max}$	
Blade twist	$\theta \leq \theta_{max}$	
Blade tip Mach no.	$M \leq M_{max}$	Limits thickness noise
Blade thickness	$h \leq h_{max}$	
Blade lift distribution	$dC_l/dx \leq S_{max}$	Limits BVI & loading noise
Ground resonance	$\lvert\Omega - \omega_{L1}\rvert < \omega_{af}$	Effective airframe constraint
Rotor/Airframe frequency coupling	$f_l \leq N\Omega \leq f_u$	

TABLE 3.- INTERACTIONS AMONG DISCIPLINES

Variable	Acoustics	Aerodyn. (Perf & Loads)	Dynamics	Structures	Fuselage Dynamics
Airfoil Dist.	S	S	W	W	W
Planform	S	S	S	S	S/W
Twist	W	S	S	W	W
Tip speed	S	S	S	S	S
Blade number	S	W	S	W	S
Stiffness	W	S	S	S	S/W
Mass dist.	W	W	S	S	S/W
Hinge offset	W	W	S/W	W	S/W

S = Strong interaction
W = Weak interaction

TABLE 4.- CANDIDATE TASK AND MISSION FOR PHASE 1 DESIGN ACTIVITY

4000 ft 95° Condition	
Aircraft gross weight	16875 lb
Installed power limit	3400 HP
V_{cruise}	140 kts
V_{max}	200 kts
g's at 120 kts	3.5
Vertical rate of climb	1000 fpm
Airframe structure	UH-60B

Other constraints and guidelines are specified in table 2.

TABLE 5.- OPTIMIZATION RESULT FOR RECTANGULAR AND TAPERED BLADES

	Reference blade	Optimum blade	
		Rectangular 30 d.v.	Tapered 42 d.v.
λ_h	1.0	1.0	1.49
f_1, Hz	12.285	12.408*	12.408*
f_2, Hz	16.098	16.056	16.066
f_3, Hz	20.913	20.968	20.888
f_4, Hz	34.624	34.546	34.678
f_5, Hz	35.861	35.502*	35.507
Autorotational inertia, lb-ft^2	517.3	517.3*	517.3*
Blade weight, lbm	98.27	95.62	92.16
Percent reduction in blade weight**	---	2.67	6.21

**-From reference blade
*-Active constraint

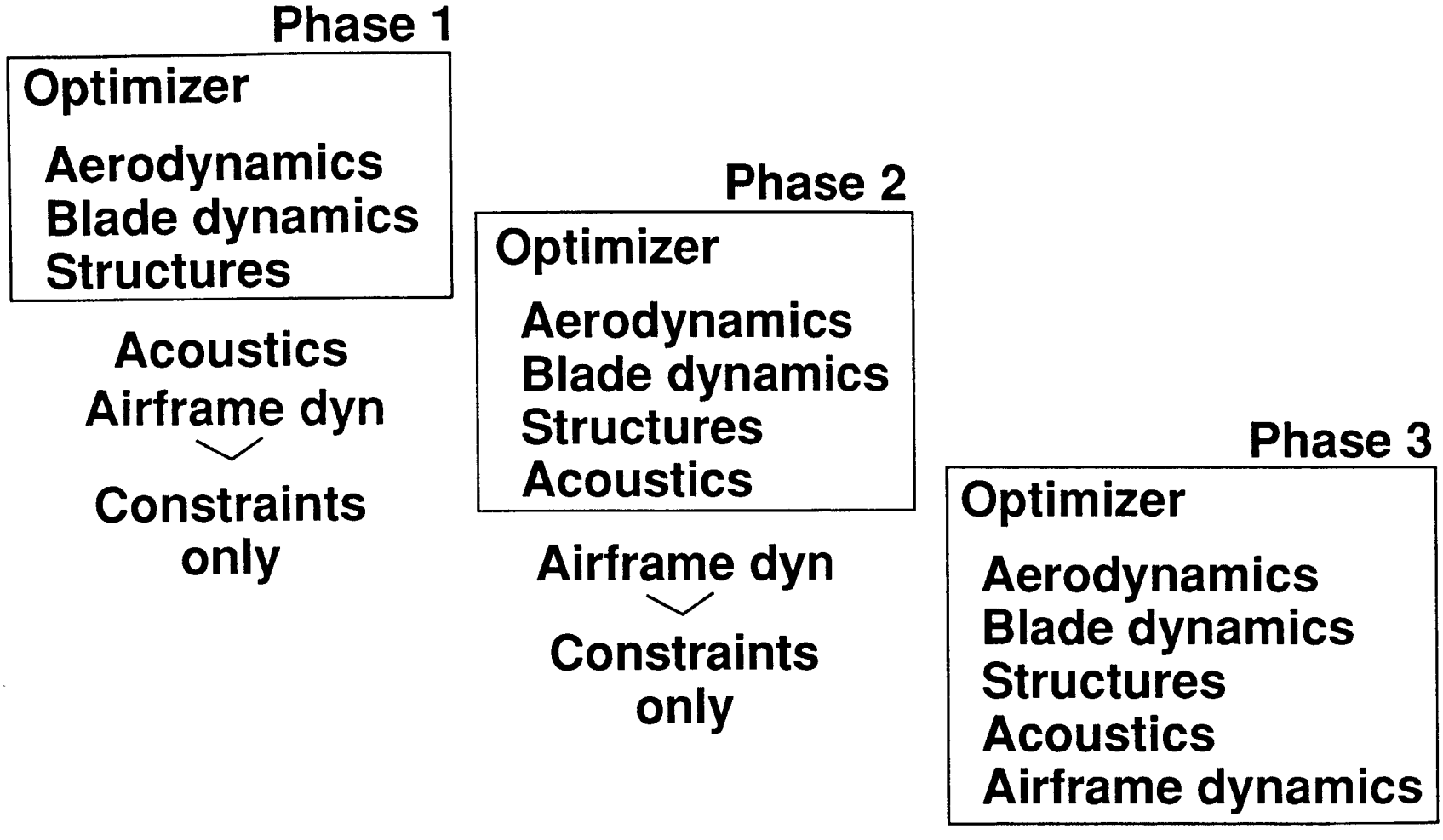

Figure 1.- Phased Approach to Development of Integrated Rotorcraft Optimization Procedures.

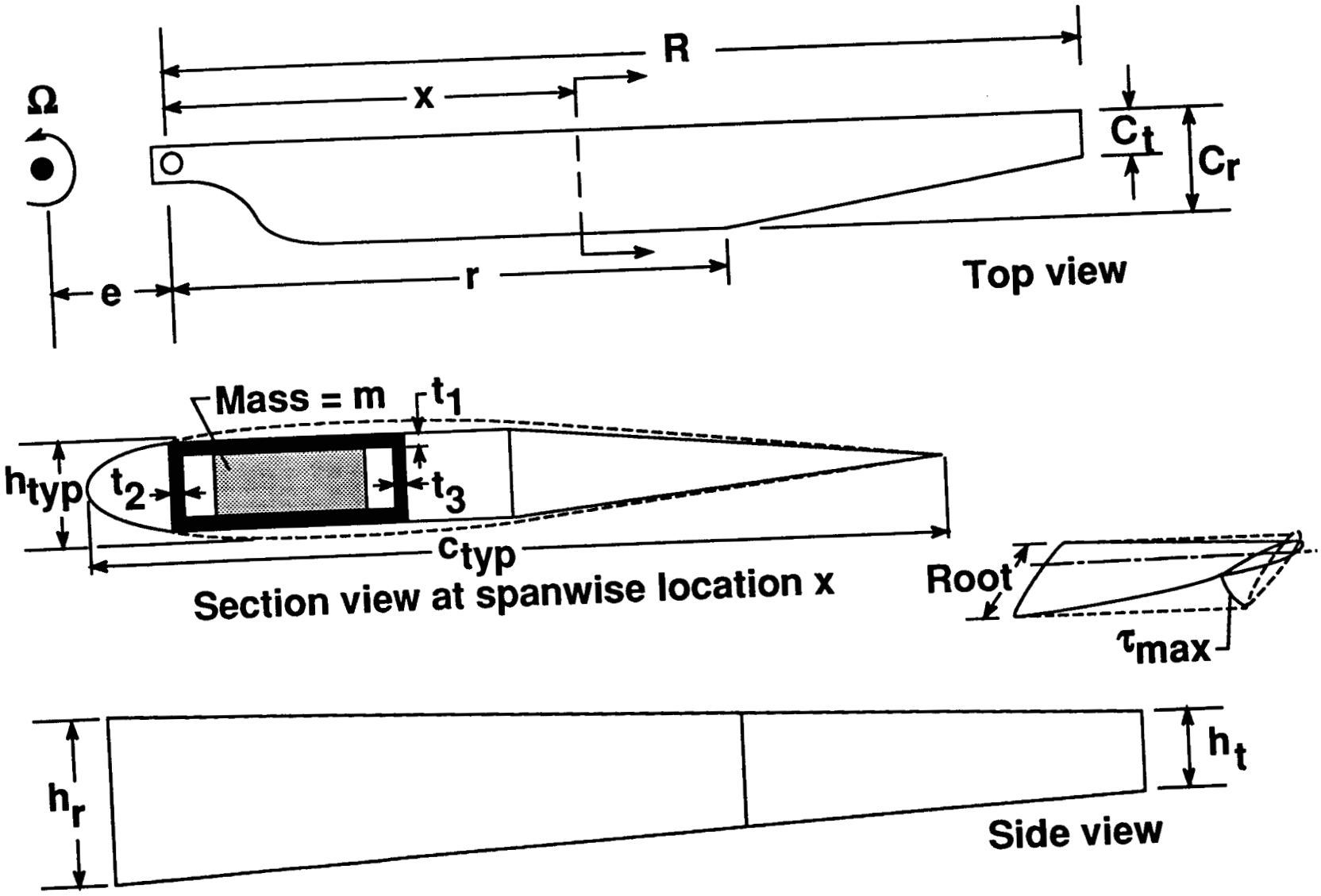

Figure 2.- Blade Model and Design Variables.

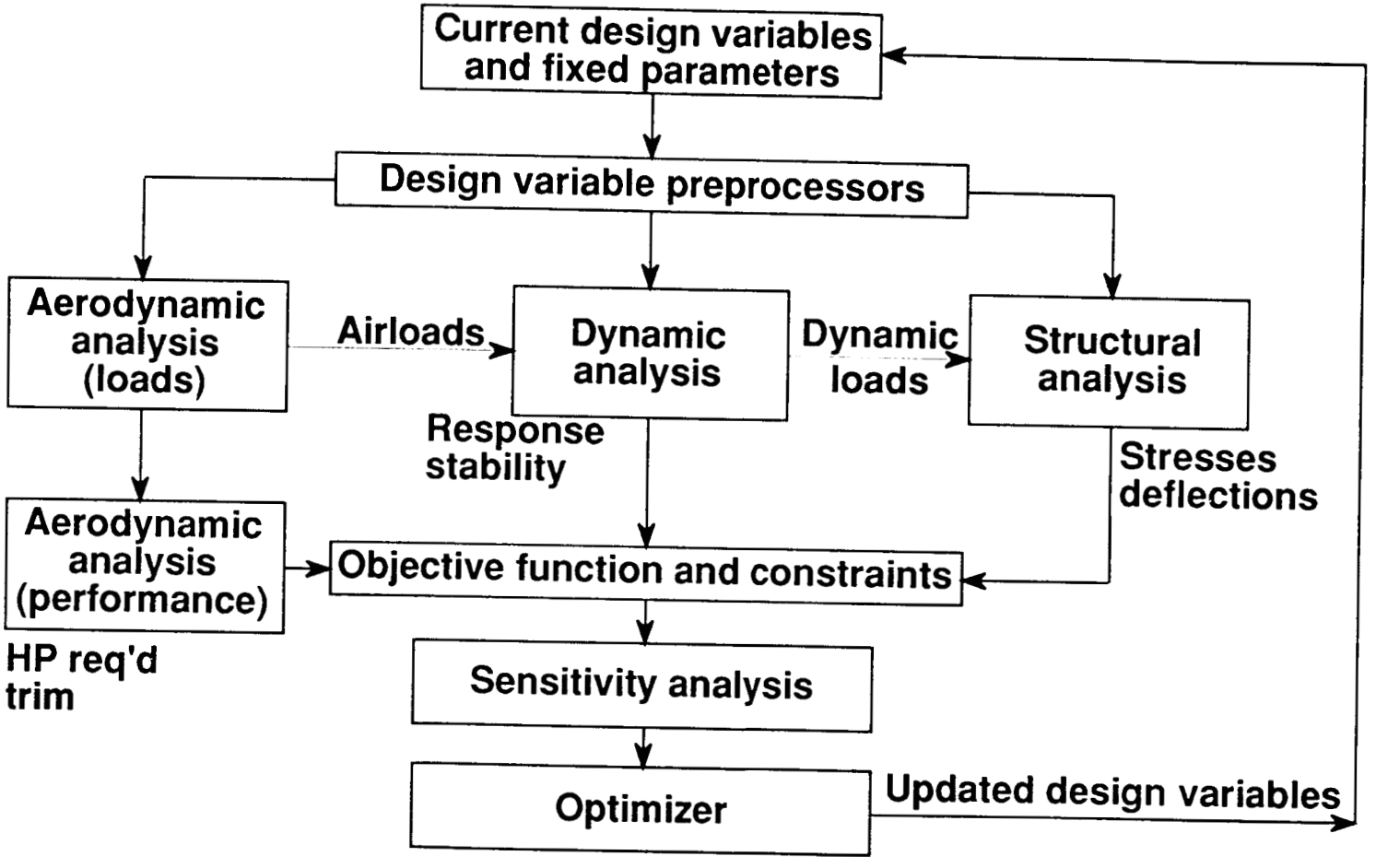

Figure 3.- Integrated Aerodynamic-Dynamic-Structural Optimization of Rotor Blades.

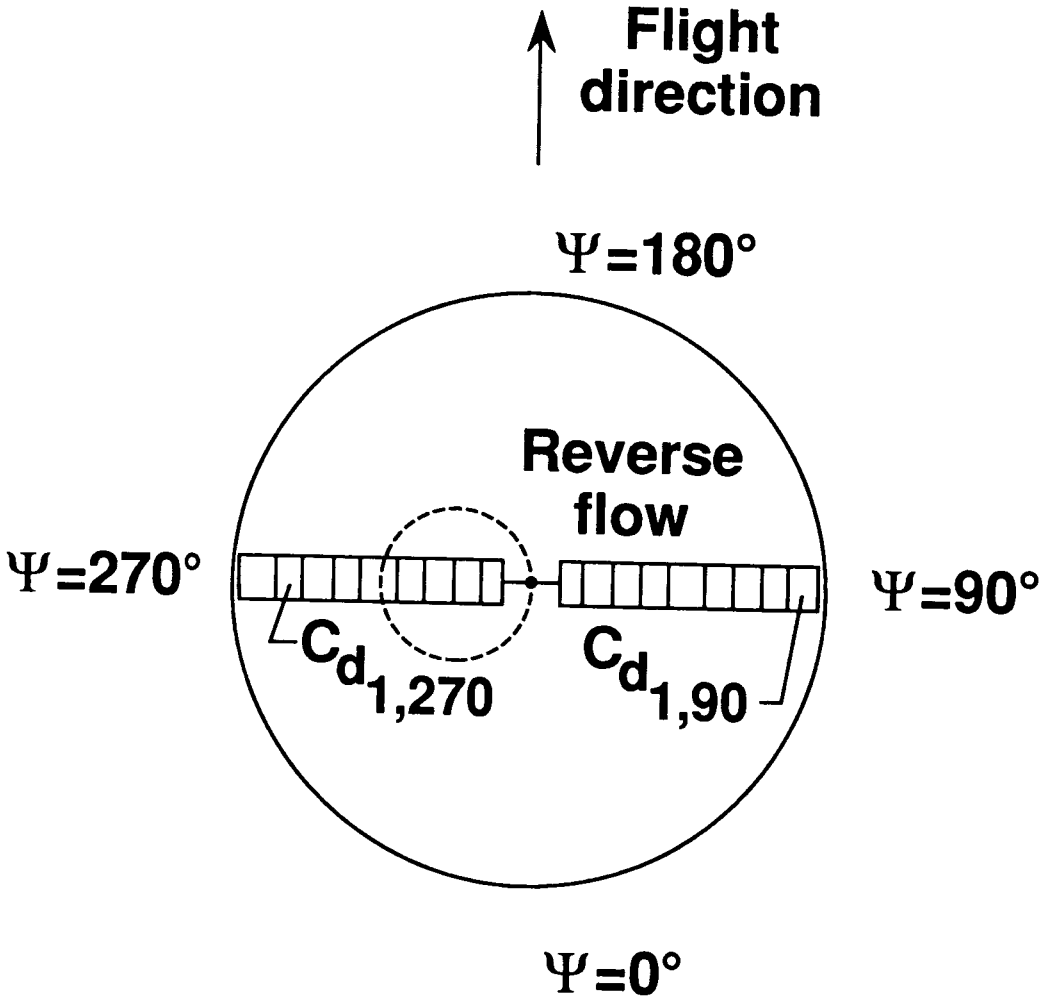

Figure 4.- Schematic Diagram Used to Establish Airfoil Section Stall Constraint.

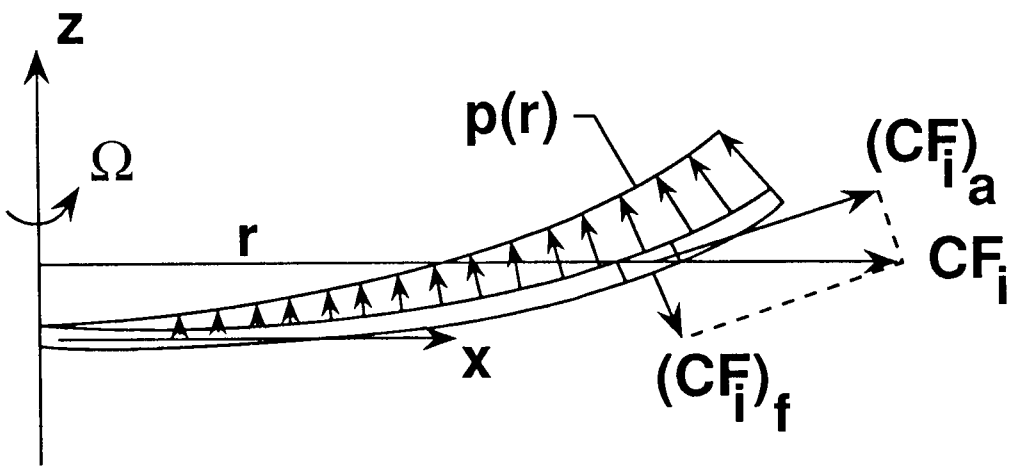

Figure 5.- Interaction of Flapwise and Centrifugal Loads Acting on Rotor Blade Model.

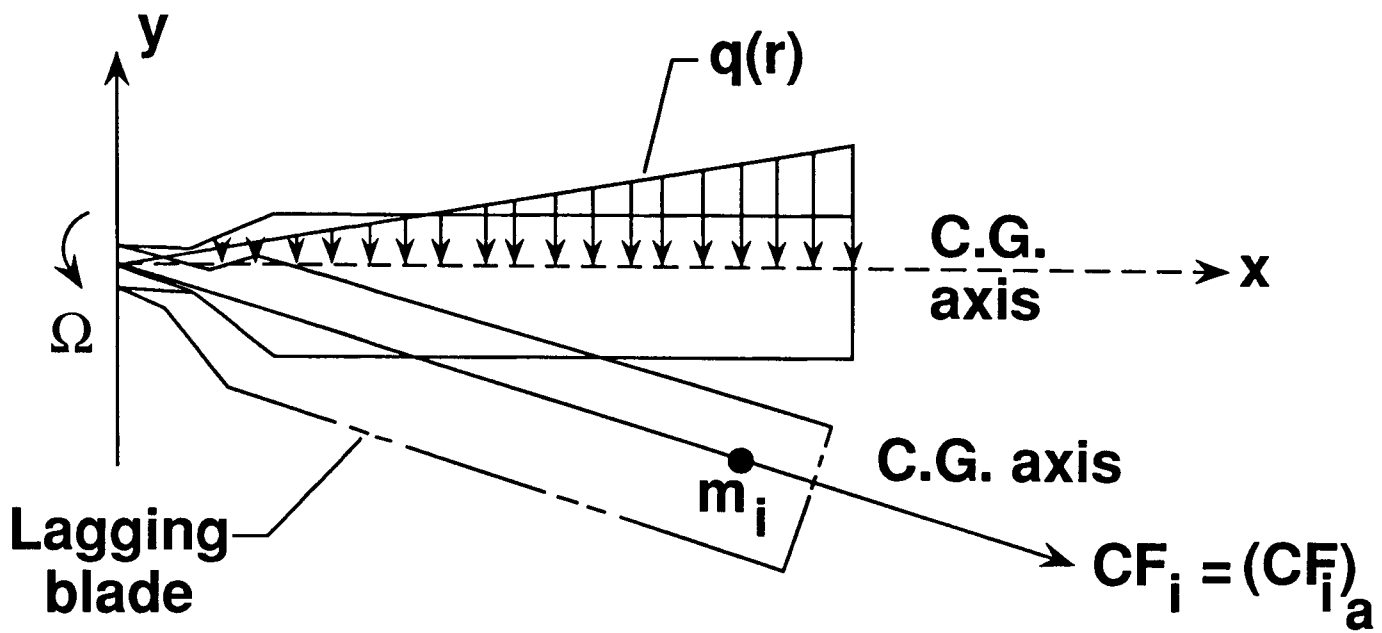

Figure 6.- Interaction of In-Plane and Centrifugal Loads Acting on a Rotor Blade Model.

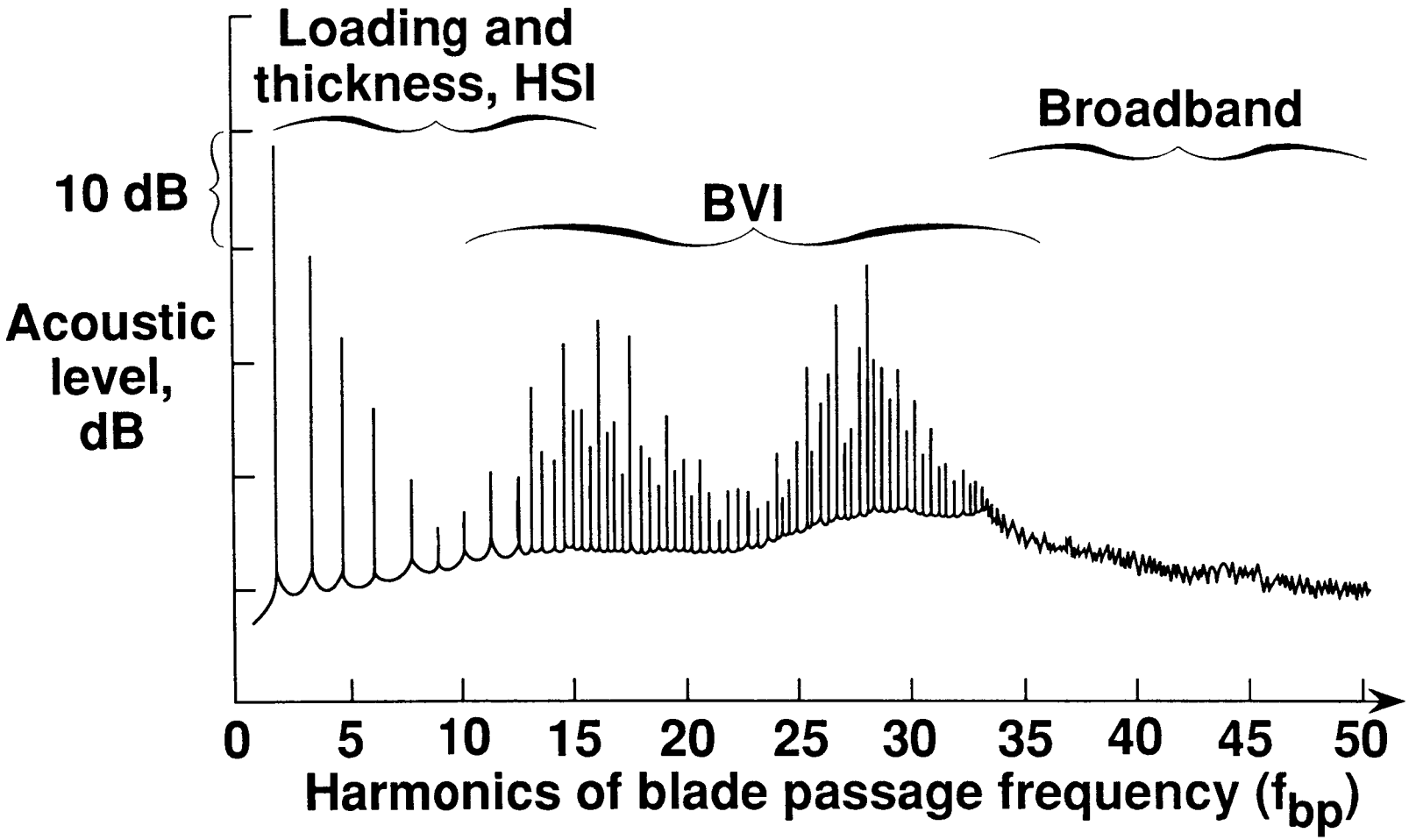

Figure 7.- Illustration of Frequency Ranges of the Major Rotor Noise Sources.

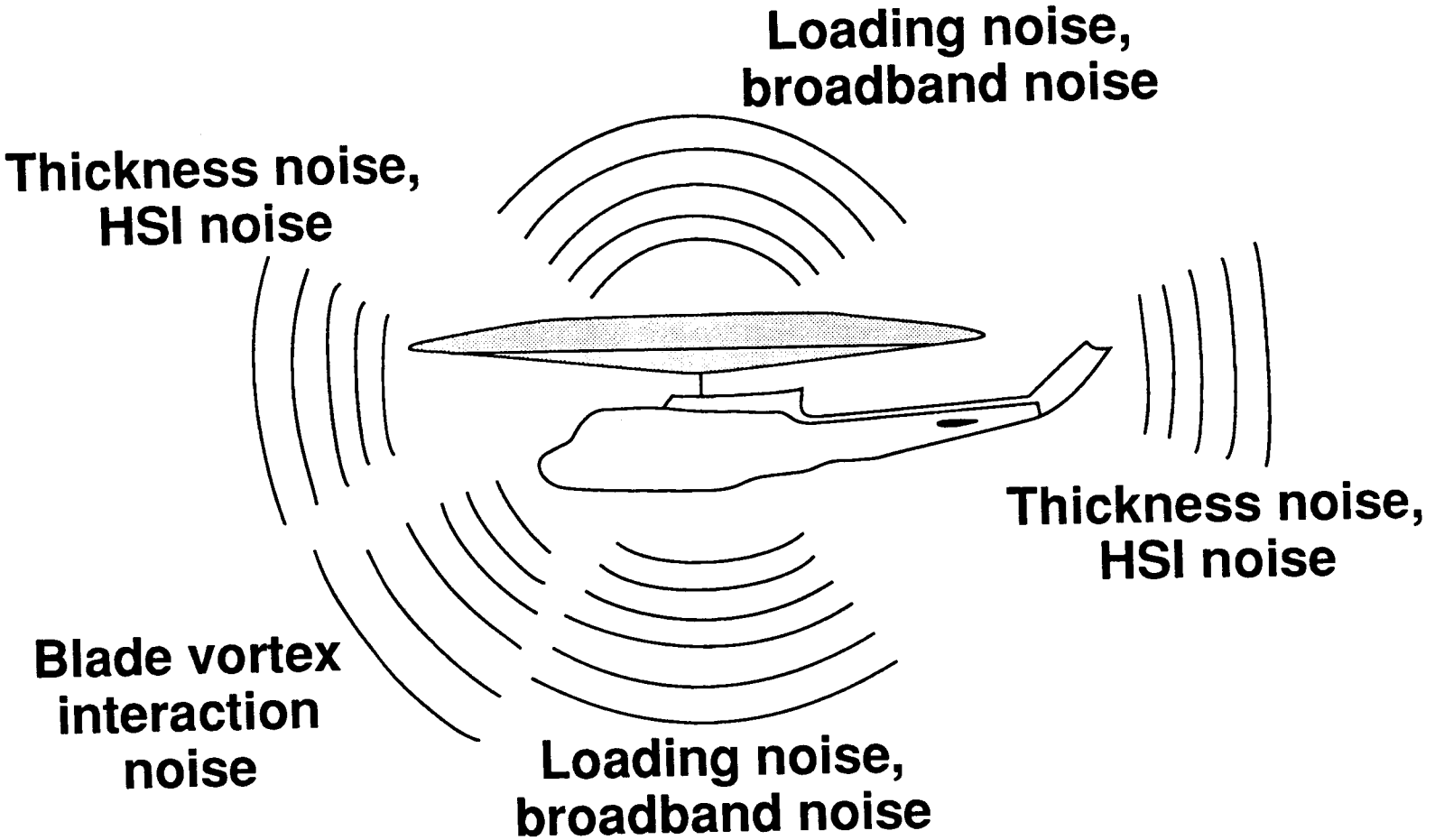

Figure 8.- Illustration of the General Directivity Patterns of the Major Rotor Noise Sources.

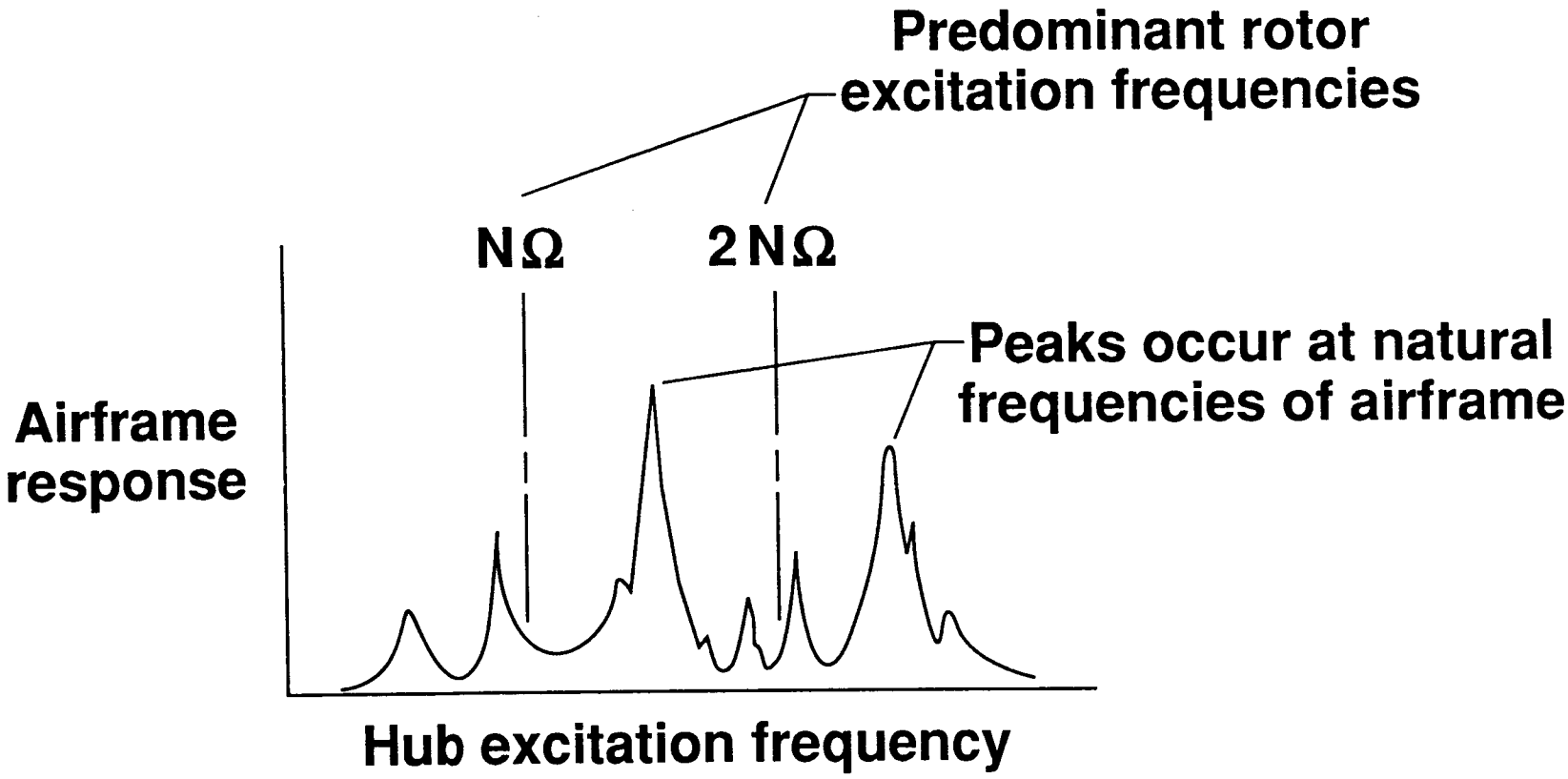

Figure 9.- Typical Variation of Airframe Response With Hub Excitation Frequency.

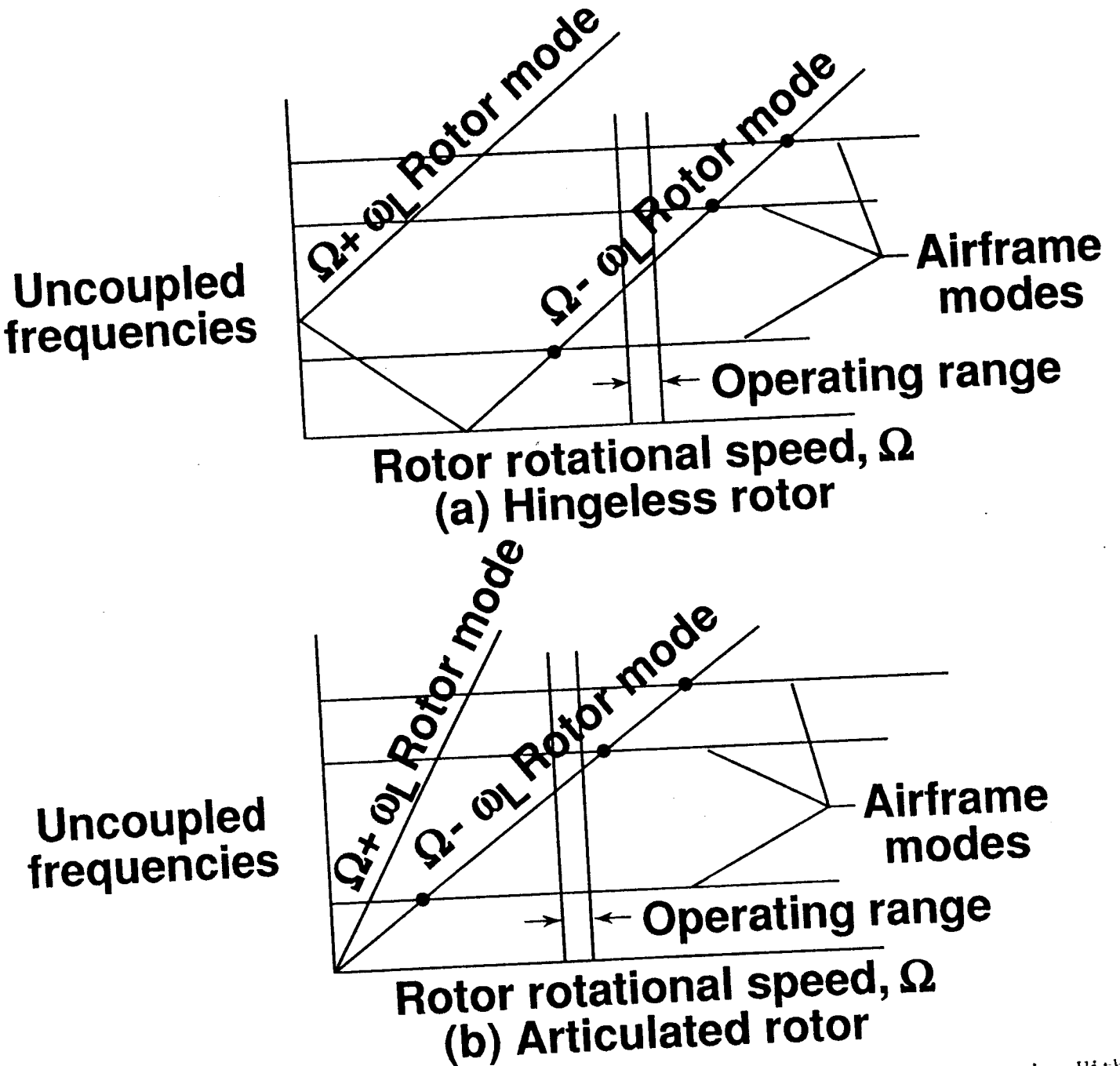

Figure 10.- Typical Variation of Uncoupled Rotor and Airframe Frequencies With Rotor Rotational Speed for Assessment of Ground and Air Resonance.

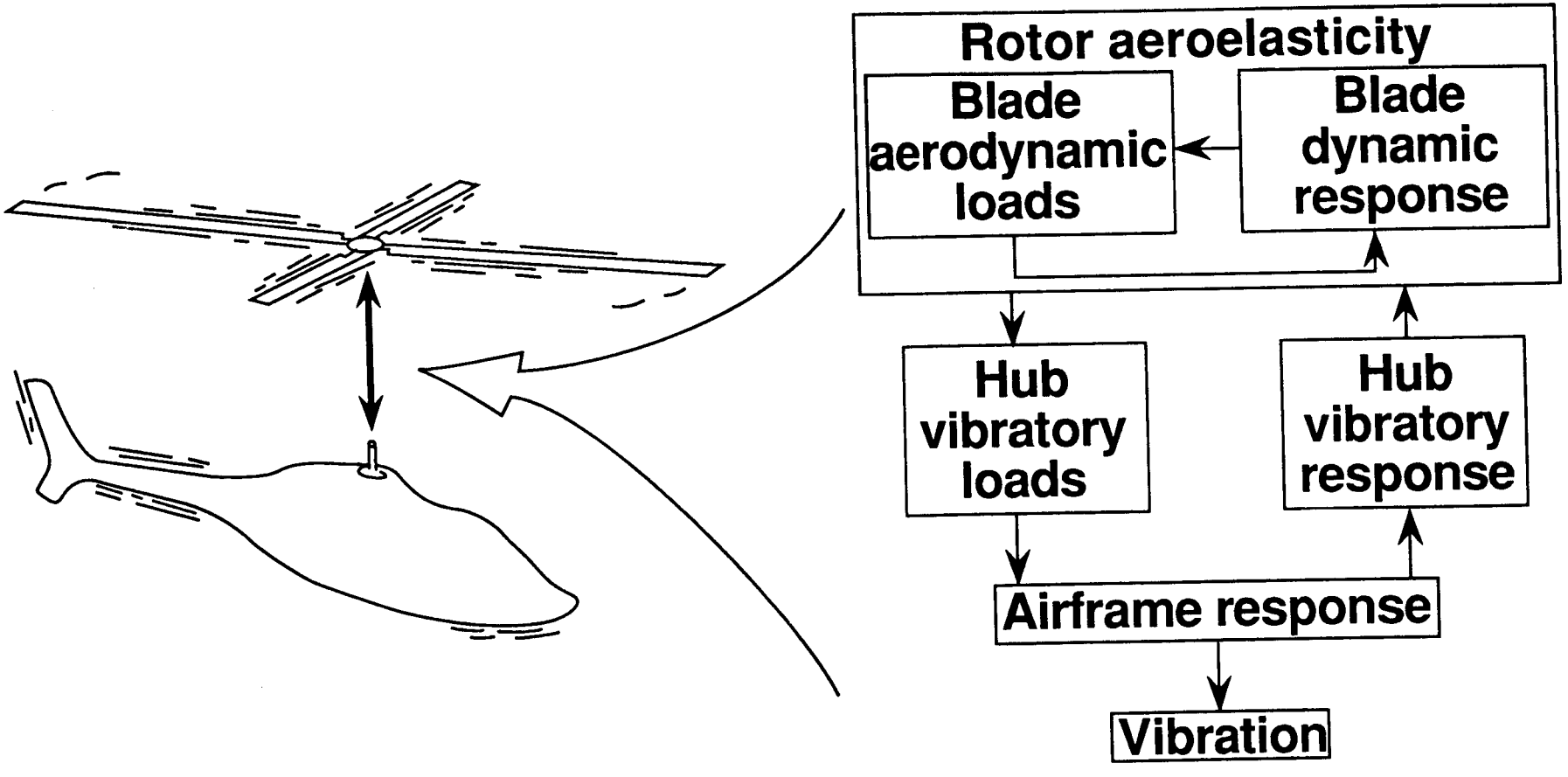

Figure 11.- A Simplified View of Rotor-Airframe Interaction in Producing Vibrations.

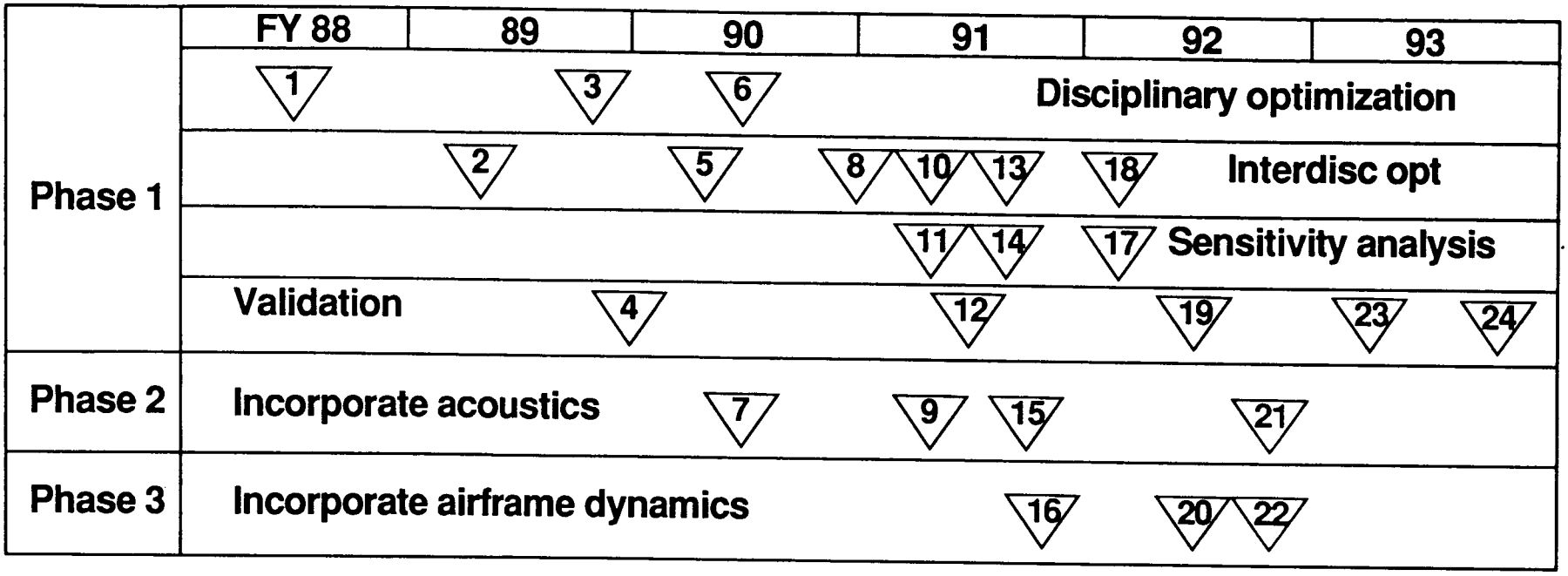

Milestones:

1 Dynamic optimization
2 Aero Load/Dyn opt
3 Performance opt
4 Apply Dyn opt to GBH-T
5 Full Aero/Dyn opt
6 Structural opt
7 Formulate Phase 2
8 Aero/Dyn/Struc opt
9 Incorporate WOPWOP code
10 Acoustics constraints
11 Aerodynamic sens analysis
12 Specs for test article
13 Airframe constraints
14 Acoustic sens analysis
15 Incorp acous sens analysis
16 Formulate phase 3
17 Airframe dyn sens
18 Complete phase 1 dev
19 Design test article
20 Rotor/AF coupling
21 Complete phase 2
22 Incorp AF sens analysis
23 Fabricate test article
24 Test article in TDT

Figure 12.- Development Schedule and Milestones for Integrated Rotorcraft Optimization.

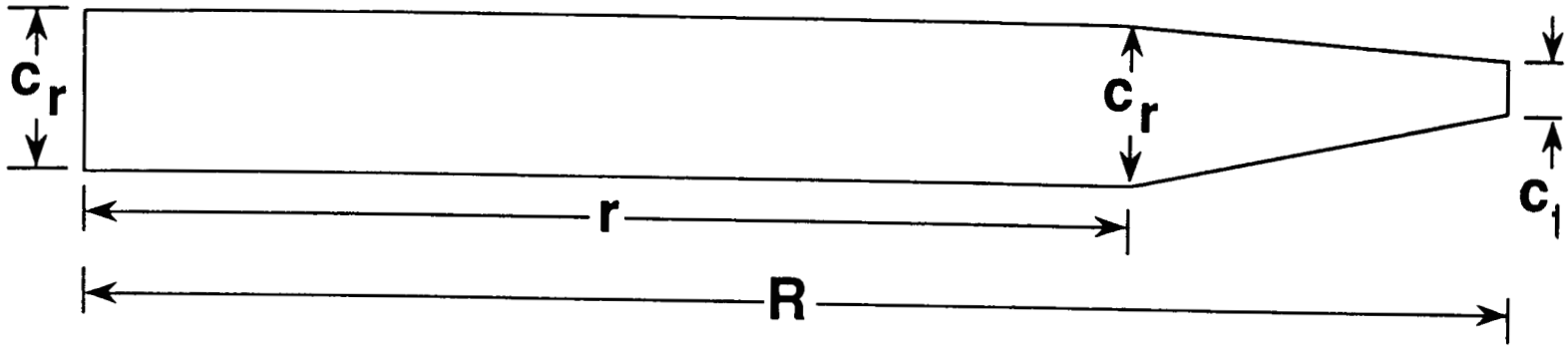

Point of taper initiation r
Root chord c_r
Taper ratio c_r/c_t

Twist

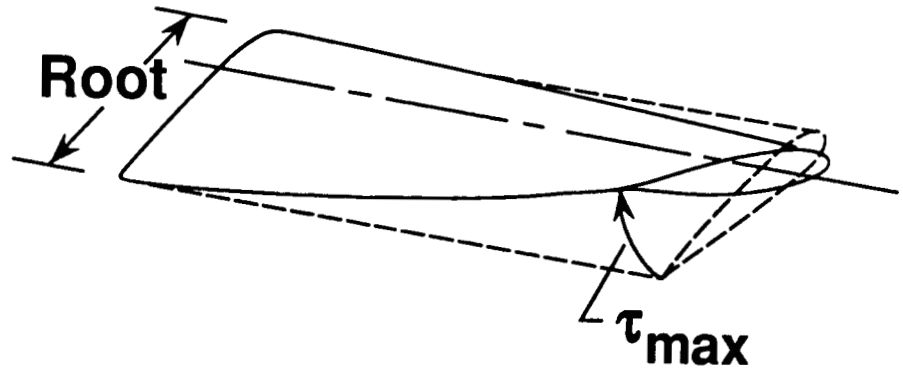

Figure 13.- Rotor Blade Design Variables for Aerodynamic Performance.

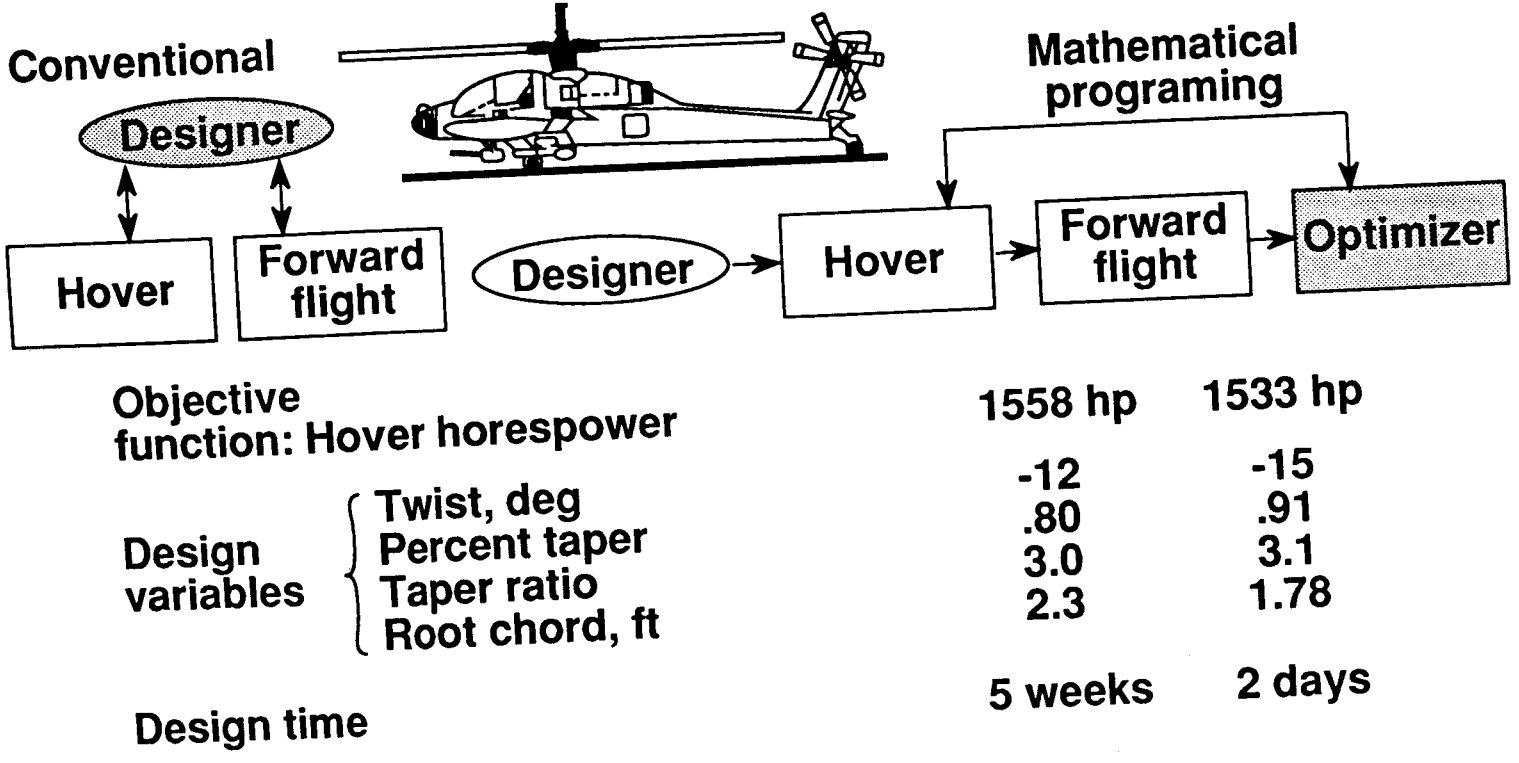

Figure 14.- Results of Aerodynamic Performance Optimization.

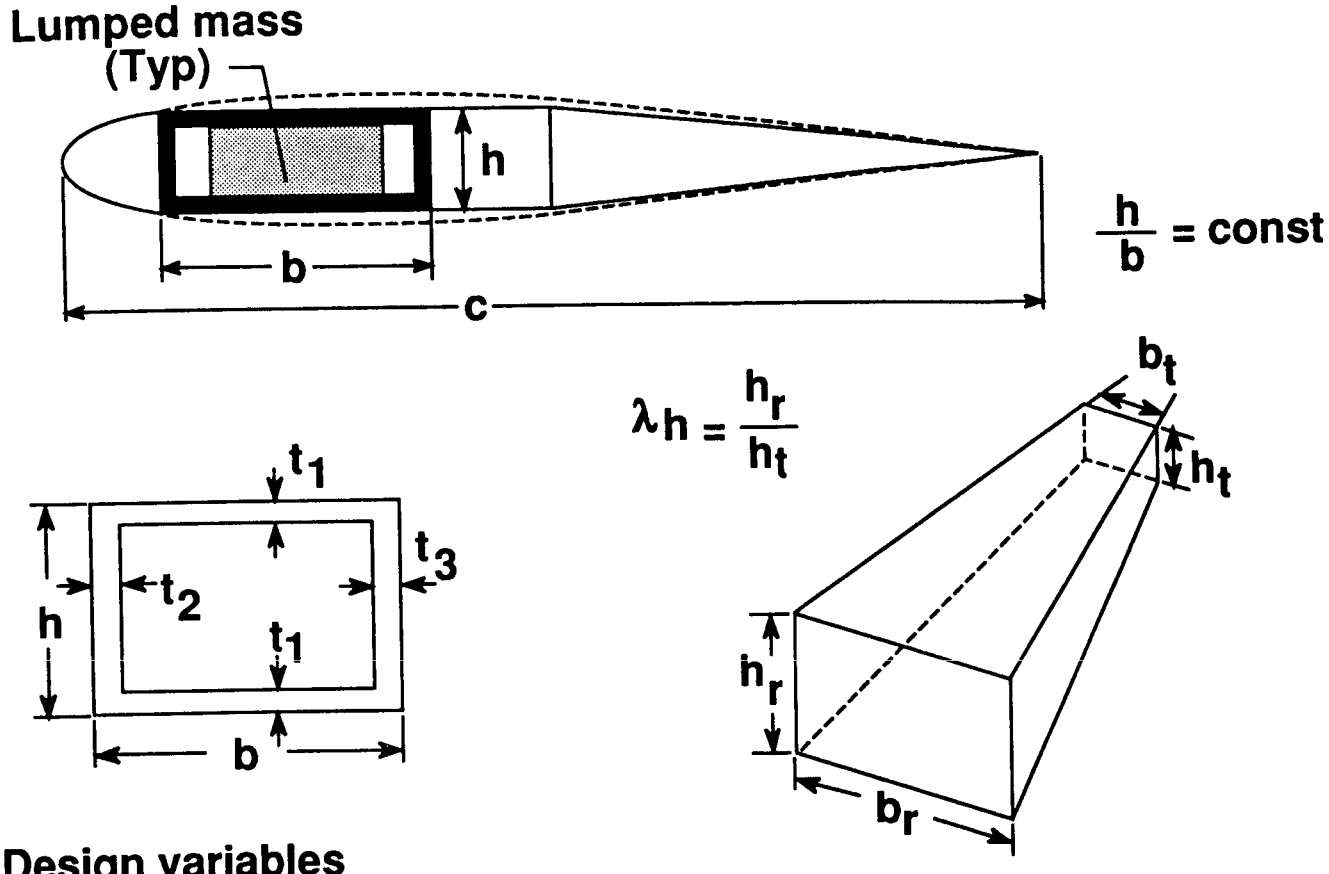

- Design variables
  - Box beam wall thicknesses, t_1, t_2, t_3 (at spanwise positions)
  - Box beam outer dimension h_r
  - Taper ratio λ_h
  - Magnitudes of lumped masses (at spanwise positions)

Figure 15.- Model and Design Variables for Dynamic Optimization Example.

- **Minimize: Blade weight W**

$$W = W_b + W_o$$

$$= \sum_{j=1}^{N} \rho_j A_j L_j + \sum_{j=1}^{N} W_{o_j}$$

W_b = box beam weight

W_o = nonstructural

- **Constraints**

Frequency $f_{k_L} \le f_k \le f_{k_U}$

$k = 1,2,...,5$ (elastic modes only)

Autorotational inertia $\sum_{j=1}^{N} W_j r_j^2 \ge \alpha$

α: minimum prescribed rotary inertia

Stress $\underbrace{\left(\sum_{j=k}^{N} M_j \Omega^2 r_j / A_k \right)}_{\sigma_k} \cdot FS \le \sigma_{max}$

Side $\phi_{i_L} \le \phi_i \le \phi_{i_U}$

ϕ_i: ith design variable

Figure 16.- Mathematical Formulation of Optimization for Dynamics.

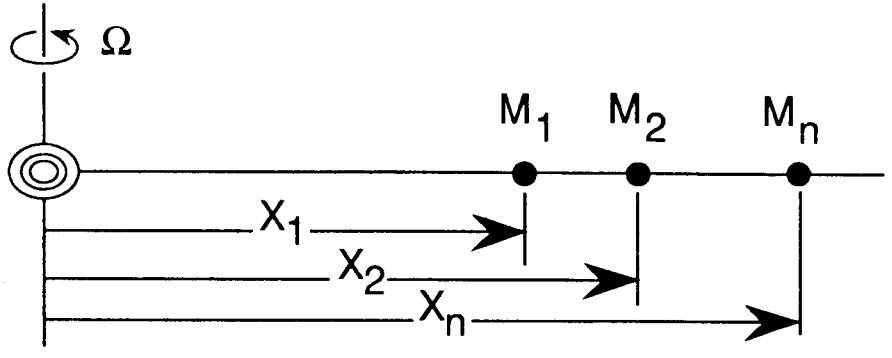

- **Design goal - Find optimum combination of masses and their locations to reduce blade root vertical shear**
- **Method - Formulate optimization procedure**
  - **Use masses and locations as design variables**
  - **Minimize -**
    - **Blade root vertical shear**
    - **Added mass**

Figure 17.- Selection of Optimum Locations of Tuning Masses for Vibration Reduction.

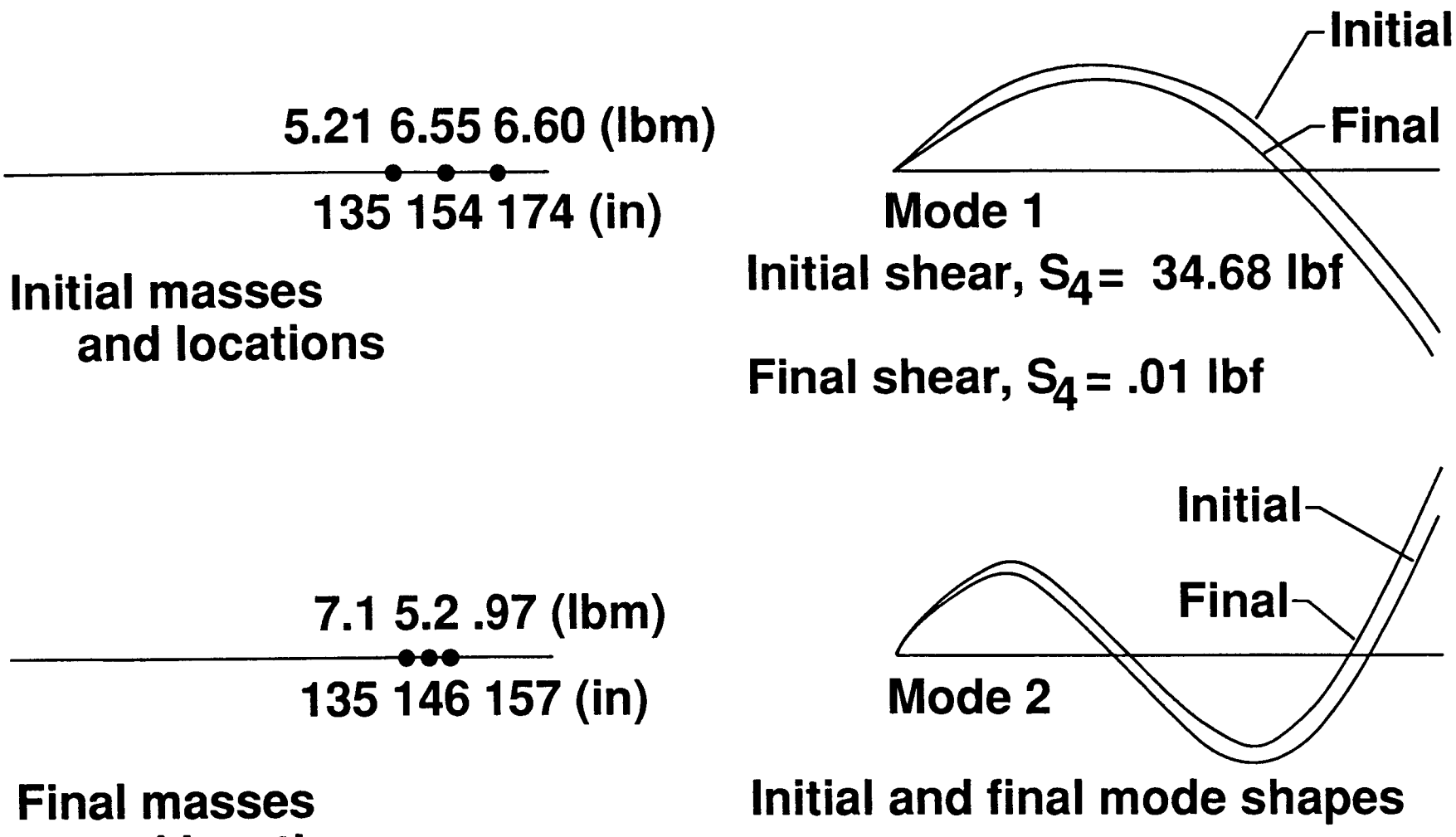

Figure 18.- Initial and Final Designs - Minimized 4/rev Vertical Shear for 2 Modes.

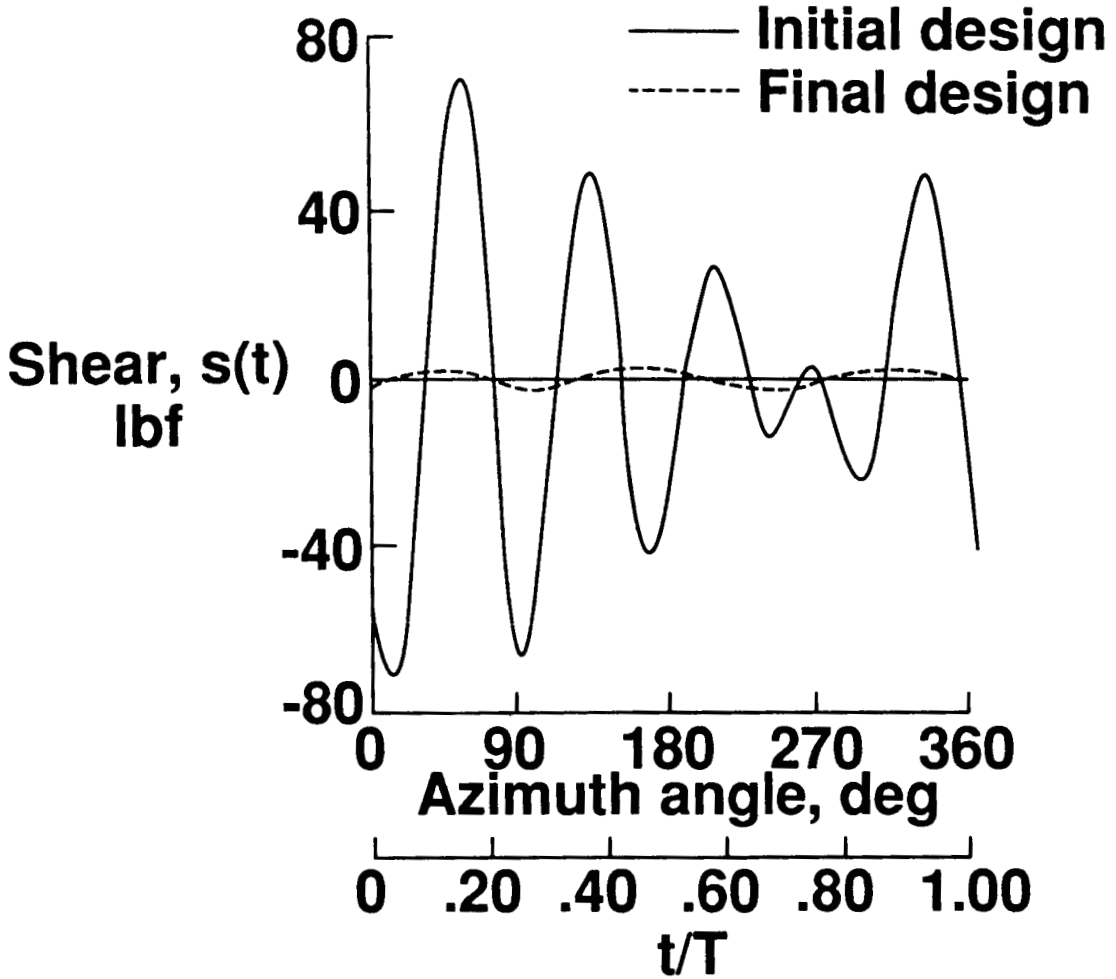

Figure 19.- Time History of Vertical Root Shear Minimized for 2 Modes/3 Harmonics.

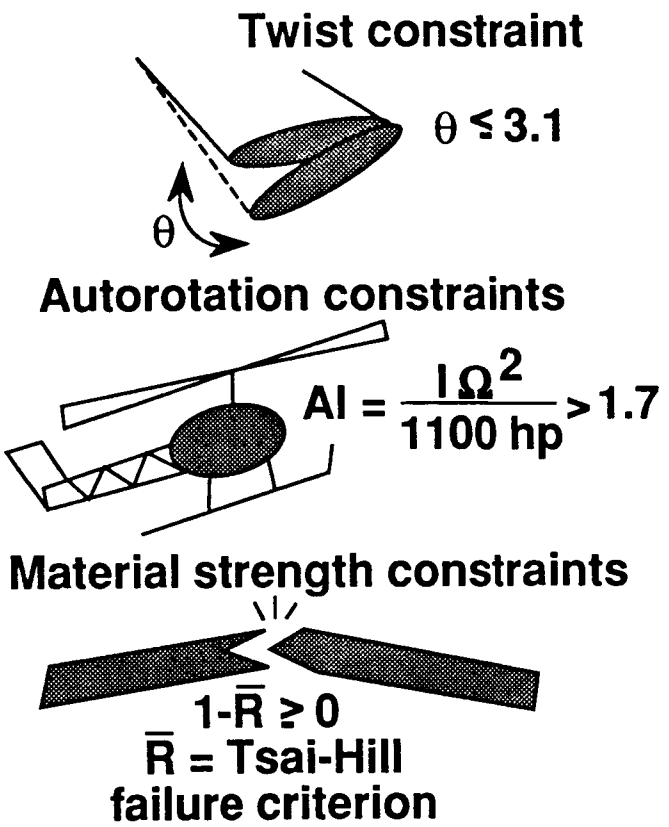

Results

Parameter	Actual UH-60A	Metal spar	Comp. spar
Spar mat.	Ti	Ti	Gr/E
Spar thick., in.	0.135	0.130	0.105
45° plys, %	---	---	20
Weight, lbs.	210	207	163
Margin (1-R̄)	---	0.103	0.000
Twist, deg.	---	0.92	2.55

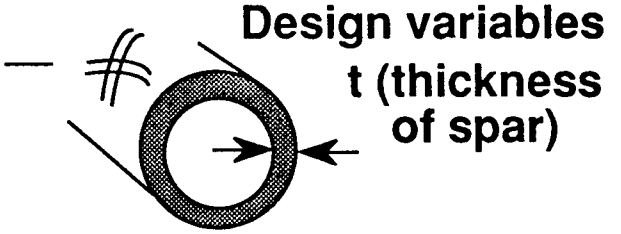

Figure 21.- Structural Optimization for Minimum Weight Rotor Blades.

- **Objective function:** Blade mass
- **Constraints:** Stress in skin and spars, twist deformation, autorotational inertia
- **Design variables:** Spar thicknesses, % of ±45° plies

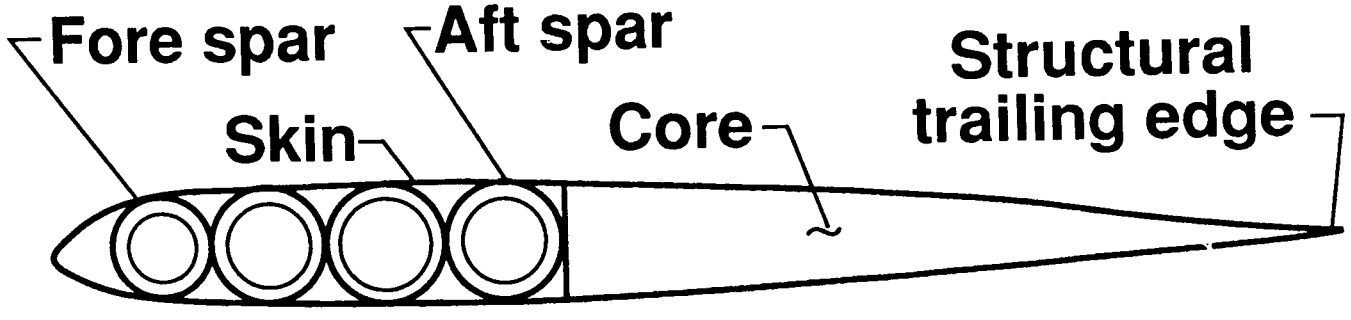

Figure 20.- Rotor Structural Optimization.